Chapter 3

Experimental Investigations of Carbon Nitrides

In this chapter an experimental investigation into carbon nitride will be presented. A range of preparation methods were employed including cathodic arc and chemical vapour deposition. These are compared to samples produced using nitrogen ion implantation into glassy carbon, magnetron sputtering and plasma-assisted CVD. Techniques involving physical vapour deposition produce films with up to 35% nitrogen in content with a primarily carbon-sp^2 structure. The average bond length of these materials is shorter than found in amorphous carbon. Carbon nitrides deposited using Chemical Vapour Deposition were diamond-like carbon materials with little or no nitrogen content. At the conclusion of this chapter a structural model for sp^2-carbon $a-$C:N is explained by nitrogen substituting into sp^2 rings to a saturation level of about one nitrogen per three atoms in the material.

3.1 Introduction

As discussed in Chapter 1, amorphous carbon nitrides are useful and versatile materials with a range of properties dictated by density, carbon sp^2 fraction, amount of nitrogen and deposition method. In this chapter the deposition and analysis of $a-$C and $a-$C:N using the unfiltered cathodic arc will be discussed in detail. In addition to room temperature investigations an *in situ* annealing experiment is presented where $a-$C:N was heated to 1000°C in a CTEM and changes in the structure monitored using EELS. The structure of the cathodic arc deposited samples are compared with samples formed by N ion implantation into glassy carbon.

Following this, Section 3.3 will describe the investigation of carbon nitrides deposited by chemical vapour deposition (CVD), including both hot-filament CVD and microwave-assisted CVD. In addition a plasma-assisted CVD carbon nitride sample deposited at another laboratory was also analysed. Section 3.4 will briefly describe the analysis of reactively-sputtered carbon nitride from another laboratory. Finally in Section 3.5, these results are compared and a structural model is proposed.

3.2 TEM Analysis of Cathodic Arc Carbon Nitride

During the course of this investigation, many $a-$C:N films were prepared using different deposition conditions. It was found that many had very similar structures and nitrogen concentrations, and so for this section two representative specimens were chosen. These were films deposited at 20 and 50 mTorr, referred to as CN20 and CN50 respectively. Table 3.1 lists the average nitrogen concentration from the whole film as measured using EELS for these samples along with other experimental data. For comparison, the corresponding data for unimplanted glassy carbon, N implanted glassy carbon[1] and cathodic arc deposited amorphous carbon ($a-$C) are also listed. As expected there is an increase in the N concentration as the N_2 gas partial pressure increased from 20 to 50 mTorr. The maximum nitrogen concentration was found to be 31% which compares well with the maximum nitrogen level (26%) found in glassy carbon films following N irradiation [1].

When viewed in a TEM, the $a-$C:N films appeared amorphous with the only crystalline material found due to the occasional presence of graphite macro-particles. This was checked by searching the electron diffraction pattern of each sample and checking that only diffuse reflections were present. The diffraction patterns of the amorphous regions were typical of amorphous materials with no strong reflections. By viewing the films in cross-section using STEM dark field imaging some features could be observed, see fig 3.1. Columnar-like features or "flakes" were found to extend a third of the thickness of the film. These features are due to either the presence of pores within the film or a variation in density within the film.

			Energy Filtered		
	EELS Analysis		Electron Diffraction		
Experimental	Nitrogen	Plasmon	1st NN	2nd NN	Bond
Data	Conc. (At. %)	(eV)	(Å)	(Å)	Angle
Glassy carbon	0	24	1.42	2.44	118°
CN50	31±2%	23	1.40	2.42	120°
CN20	20±2%	24	1.42	2.44	118°
Implanted glassy carbon[a]	(26±2%) [b]				
$a-$C	0	24	1.48	2.52	117 °

Table 3.1: A list of the experimentally measured nitrogen concentration, plasmon energy and reduced density function information (nearest neighbour distances (NN) and bond angles) for (a) glassy carbon (b) two cathodic arc deposited (c) glassy carbon implanted with 50keV nitrogen ions to a dose of 1×10^{18} cm^{-2} and (d) cathodic arc deposited amorphous carbon (a-C) in argon ambient.

[a] Glassy carbon implanted with 50keV N^+ to a dose of 1×10^{18} cm^{-2}.
[b] Calculated using Rutherford Back Scattering.

Figure 3.1: A cross-sectional dark field STEM image of an $a-$C:N film deposited using cathodic arc in dark field mode with a selected area aperture.

In order to determine whether there was a variation in the nitrogen concentration with depth into an $a-$C:N film, samples were analysed using EELS line scans available in the STEM. The elemental concentrations were extracted from the EELS spectra using the techniques described in Section 2.5 on page 50. Fig (3.2) shows a linescan through the films from the surface to the "substrate". In the figure, the film had broken away from the substrate so leftmost is an epoxy/film interface while to the right is the film/gap interface. Fig (3.2) shows that there is minimal variation in carbon and nitrogen with depth. In addition to nitrogen and carbon, a small amount of oxygen was found at film interfaces. This is shown by the oxygen signal to the left of fig (3.2), and a small peak revealing oxygen originally adsorbed onto the substrate, now present at the interface..

3.2.1 Low-loss or Plasmon Analysis

The plasmon energies were measured from the low-loss EEL spectra for the cathodic arc deposited samples are shown in Table 3.1. There is no significant difference in the plasmon energies for the samples analysed. Fig (3.3) shows an EELS linescan measurement of plasmon energy and t/λ ratio. There is no appreciable variation in the plasmon energy (an indicator of density) through the film.

Since nitrogen has more valence electrons than carbon and the plasmon energy is proportional to the square root of electron density [2], the nitrogen containing samples for the same atom density should have a higher plasmon energy. Therefore the similar plasmon energy measured from samples with and without nitrogen indicates that the nitrogen rich material consists of a lower density network than the a-C.

3.2.2 Structural and Elemental Analysis at elevated temperatures.

To further investigate the structure of $a-$C:N, a sample of $a-$C:N was heated to temperatures of up to 1000 °C in a CTEM using a heating holder. The aim of this *in situ* annealing experiment was to monitor the possible evolution of small crystallites of carbon nitride material with a different stoichiometry to the bulk material. At each annealing temperature, the film was carefully examined for the presence of crystallites. At anneal temperatures of 800°C and 1000°C graphite crystallites were observed to

form near the edges of the carbon nitride film. However, over the whole annealing temperature range, there was no evidence for the formation of crystallites containing more nitrogen than the amorphous matrix as measured using EELS.

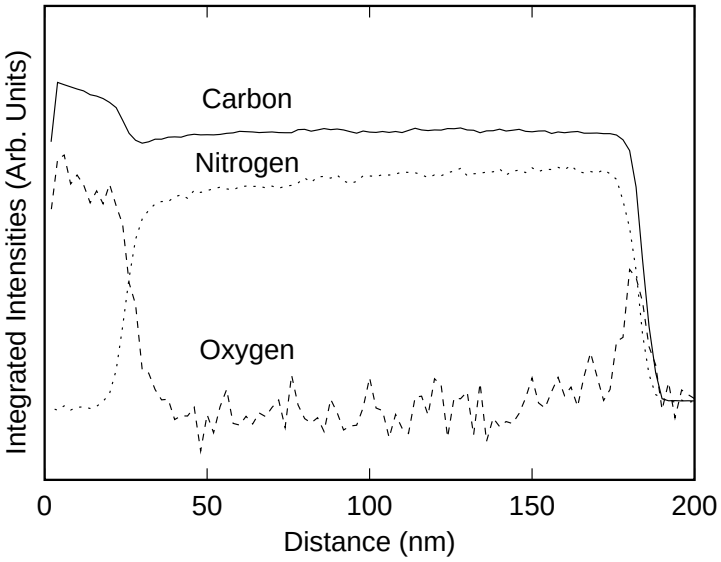

Figure 3.2: EELS Line-scan of cathodic arc deposited $a-$C:N on glassy carbon sample showing variation of carbon, nitrogen and oxygen concentration across the width of the sample. Integrated intensites were calculated over a 40–50eV integration window on non-background subtracted core-loss spectra.

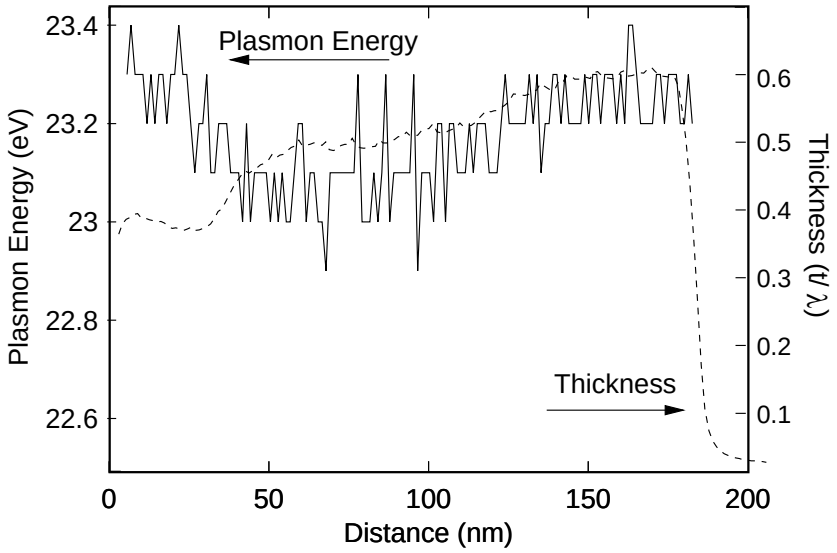

Figure 3.3: EELS linescan of cathodic arc deposited $a-$C:N sample onto a glassy carbon substrate showing variation of plasmon and t/λ with depth.

In fig (3.4) the nitrogen concentration is shown as calculated from the EELS spectra for the carbon nitride film as a function of annealing temperature. The error bars on the plot are indicative of the variation in the nitrogen concentration from a number of measurements from different positions on the specimen. The as-deposited material was found to have a nitrogen concentration of 31%. As is apparent from the figure, the nitrogen concentration is significantly affected by annealing, decreasing rapidly with increasing temperature. Even an anneal temperature of 200 °C is sufficient to reduce the nitrogen concentration from 31 to 27%. This initial drop in nitrogen can be explained by the presence of a significant proportion of loosely bound nitrogen desorbing from within the structure.

Between 200°C and 400°C the nitrogen concentration remains at a relatively constant level. For anneal temperatures between 400°C and 1000°C the nitrogen concentration decreases steadily from 27 to 9%.

The plasmon energies measured from low loss EELS spectra are plotted in fig (3.5) as a function of anneal temperature. The plasmon energy remains relatively constant at a value of approximately 22·8 eV for temperatures below 400°C. Above 400°C, the plasmon energy decreases rapidly to a value of approximately 21·4 eV for an anneal temperature of 800°C. The plasmon energy is proportional to the square root of electron density within the film. Since nitrogen has more valence electrons than carbon the decrease in plasmon energy may be partly explained by the loss of nitrogen during annealing. However, the relatively constant level of the plasmon energy for anneal temperatures up to 400°C is not consistent with this explanation since there is a large decrease in nitrogen concentration over the same temperature range.

The behaviour of the plasmon energy with anneal temperature may reflect the annealing kinetics of the carbon-nitride film. Annealing studies of amorphous carbon materials [3, 4] have revealed that at a temperature of approximately 400°C the bonding within the amorphous carbon structure begins to relax to form graphite-like six membered rings. The process continues for anneal temperatures up to approximately 1000°C, where the amorphous carbon film is transformed into poly-crystalline graphite. Therefore the reduction in plasmon energy observed in the carbon nitride films for an anneal

temperature above 400°C logically indicates the beginning of a similar graphitisation process.

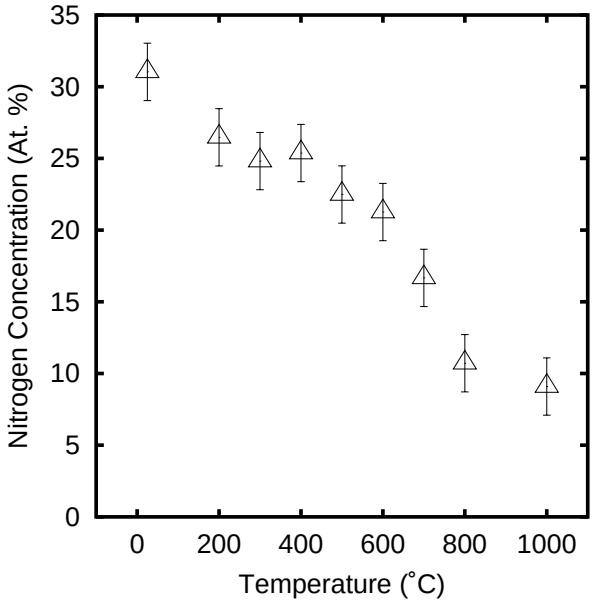

Figure 3.4: The variation of nitrogen concentration during annealing for a carbon nitride film following annealing to temperatures of 1000°C.

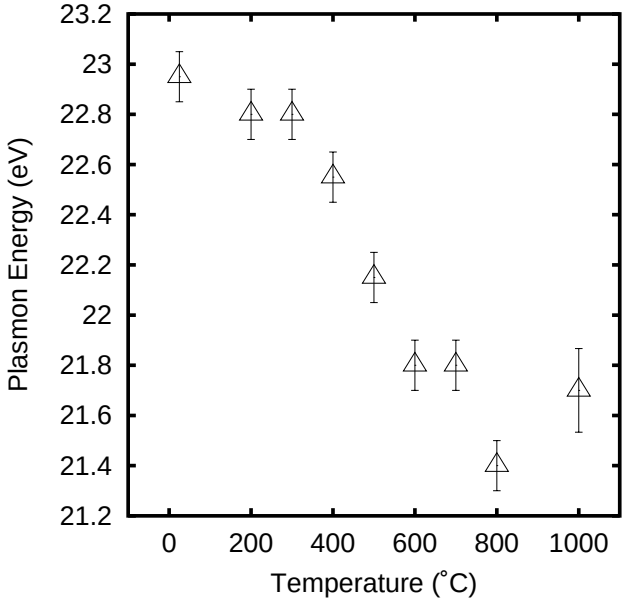

Figure 3.5: The change in plasmon energy following annealing of carbon nitride film to temperatures of 1000°C.

3.2.3 Carbon K-Edge ELNES

The graph in fig (3.6) shows the background-subtracted carbon K-edges for the $a-$C:N films deposited at 20 and 50mTorr (referred to as CN20 and CN50 respectively) and the a-C deposited in 50mTorr of argon gas. The shape of EEL edges provides structural information on the atomic environment of the absorbing atom.

The main feature of each carbon K-edge is the broad peak at 300eV, mainly due to 1s – σ^* transitions. The sharp peak at 284eV is found in sp and sp^2-bonded carbon and is a result of 1s – π^* transitions. The 1s – π^* peak in glassy carbon is relatively intense and reflects the predominance of sp^2 bonding. This peak is less defined in the a-C sample possibly due to the presence of bond angle disorder resulting from five- and seven-membered rings [5]. The sharpness of the 1s – π^* feature of both $a-$C:N materials is similar to that seen in glassy carbon suggesting a similar graphite-like sp^2 structure.

The amount of sp^2 bonded carbon does not vary significantly with depth of the film as shown in fig (3.7) indicating the film is homogeneously bonded.

3.2.4 Nitrogen K-Edge ELNES

The plots in fig (3.8) shows the nitrogen K-edges from the CN20 and CN50 cathodic arc deposited materials, normalised and background subtracted. From fig (3.8) the nitrogen K-edges appear similar to the carbon K-edges, as both contain the 1s – π^* feature. The identification of this peak as 1s – π^* is supported by IR analysis (See Section 3.2.9) and XANES analysis by Jiménez *et al.* [6], Bhattacharyya *et al.* [7] and Shimoyama *et al.* [8]. This feature indicates that the nitrogen and carbon are bonded in a similar sp^2 configurations [9], although the resolution is not sufficient to distinguish between possible types, as did later experimental XANES studies [7, 6]. The nitrogen concentration in the film is determined from the carbon and nitrogen K-edges (listed in Table 3.1) shows that the concentration of nitrogen in the cathodic arc samples increases with the nitrogen gas partial pressure.

Interestingly, the nitrogen K-edges appear similar to the carbon K-edges, as both con-

tain the $1s - \pi^*$ feature in a similar proportion to the 1s – σ^* peak. This indicates that the nitrogen atoms (like the carbon atoms) are bonded in predominantly sp^2 configurations.

The amount of π-bonded nitrogen does not vary significantly with depth of the film as shown in fig (3.7), indicating the film is homogeneously bonded.

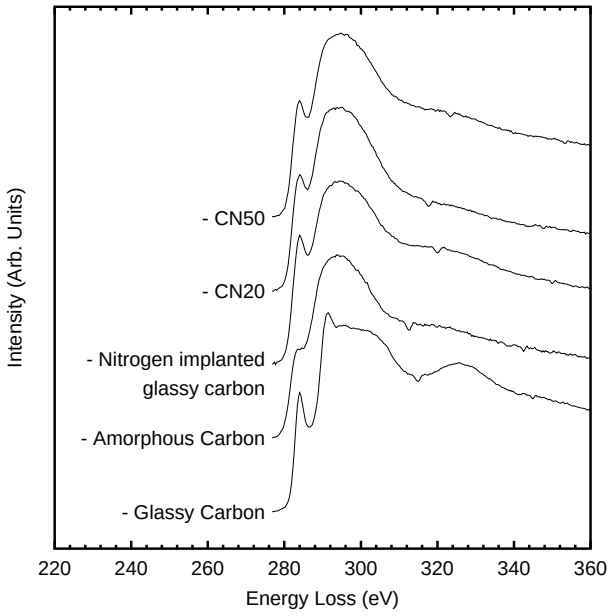

Figure 3.6: The background-subtracted carbon EELS K-edge from (a) glassy carbon, (b) cathodic arc deposited a-C with nitrogen ambient, (c) 50keV nitrogen implanted glassy carbon to dose of 1×10^{18} N cm^2,(d) cathodic arc deposited carbon nitride materials at CN20 and CN50

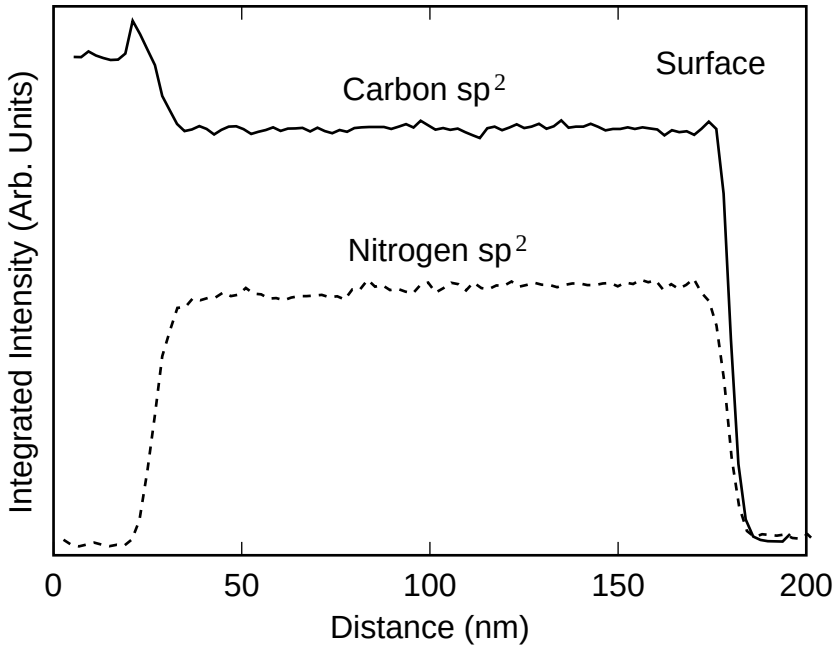

Figure 3.7: EELS Line-scan of cathodic arc deposited $a-$C:N sample on glassy carbon sample showing variation of carbon and nitrogen sp^2 fraction across the width of the sample.

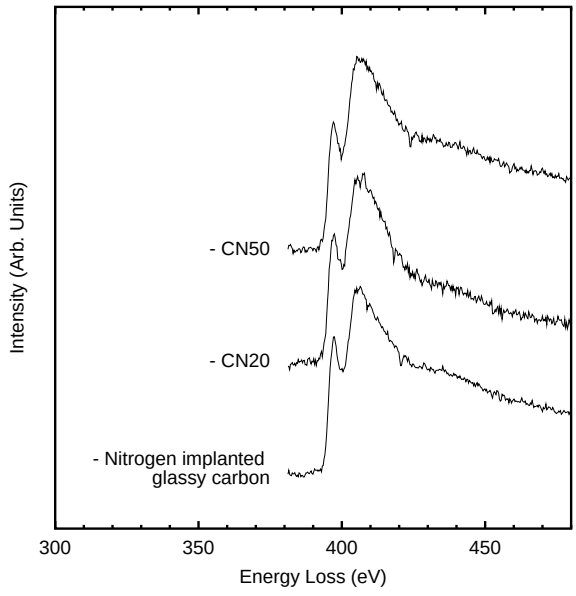

Figure 3.8: The nitrogen EELS K-edge (background subtracted) from (a) 50keV nitrogen implanted glassy carbon (Implanted Carbon) to dose of 1×10^{18} Ncm^{-2}, (b) cathodic arc deposited carbon nitride materials CN20 and CN50.

3.2.5 Variation Carbon and Nitrogen K Edge ELNES at elevated temperature.

The EELS spectra in fig (3.9) are the background-subtracted carbon K-edges for a sample of $a-$C:N film following annealing to temperatures of 200°C, 600°C and 1000°C. The carbon K-edge of glassy carbon at room temperature has also been included for comparison.

The 1s – π^* peak from the carbon nitride film annealed at 600°C shows an apparent reduction in sharpness when compared to the other spectra. This broadening of the 1s – π^* peak may be explained by a shift or splitting caused by a change in the dominant bonding type present. A range of 1s – π^* peak positions are possible depending on the exact bonding configuration [10]. For example the 1s – π^* peak position is found to increase with increasing atomic number due to stronger-bound π^* orbits. For this reason, C = C bonds are expected to have a lower peak position than C = N bonds. Therefore the broadening of the $1s-\pi^*$ peak indicates a change in the dominant bonding type from sp^2 carbon-nitrogen to sp^2 carbon-carbon as the film graphitises.

At an anneal temperature of 1000 °C, the $a-$C:N films develop a sharp π^* peak, a flatter $1s$ – σ^* peak and the graphite-like extended fine structure peak. These changes in the edge shape can be explained by the partial graphitisation – a conversion of sp^3 to sp^2 carbon atoms in the film at this temperature.

In fig (3.10) the background-subtracted nitrogen K-edges from the as-deposited $a-$C:N film and following annealing to temperatures of 200°C, 600°C and 1000°C. The only significant change in edge shape following annealing is a decrease in the intensity of the nitrogen 1s – π^* feature. This decrease in 1s – π^* intensity occurs as the nitrogen concentration also decreases (see fig (3.10)).

A study by Davis *et al.* [11] of the structure of $a-$C:N deposited using a filtered cathodic arc has also shown that the nitrogen 1s – π^* feature decreases in intensity with decreasing nitrogen levels. This result was explained by a change in nitrogen bonding from sp^2 to sp^3. In this annealing experiment, the decrease in the nitrogen 1s – π^* fea-

ture probably also corresponds to a change in nitrogen bonding as the nitrogen atoms are forced out of carbon-nitrogen sp^2 bonds as graphitisation occurs.

The reduction in nitrogen concentration with temperature shown in fig (3.4) can be explained by the graphitisation of the structure as evident in the carbon K- edge structure shown in fig (3.9). As the carbon atoms in the film arrange themselves into graphitic rings, nitrogen is driven out of the structure.

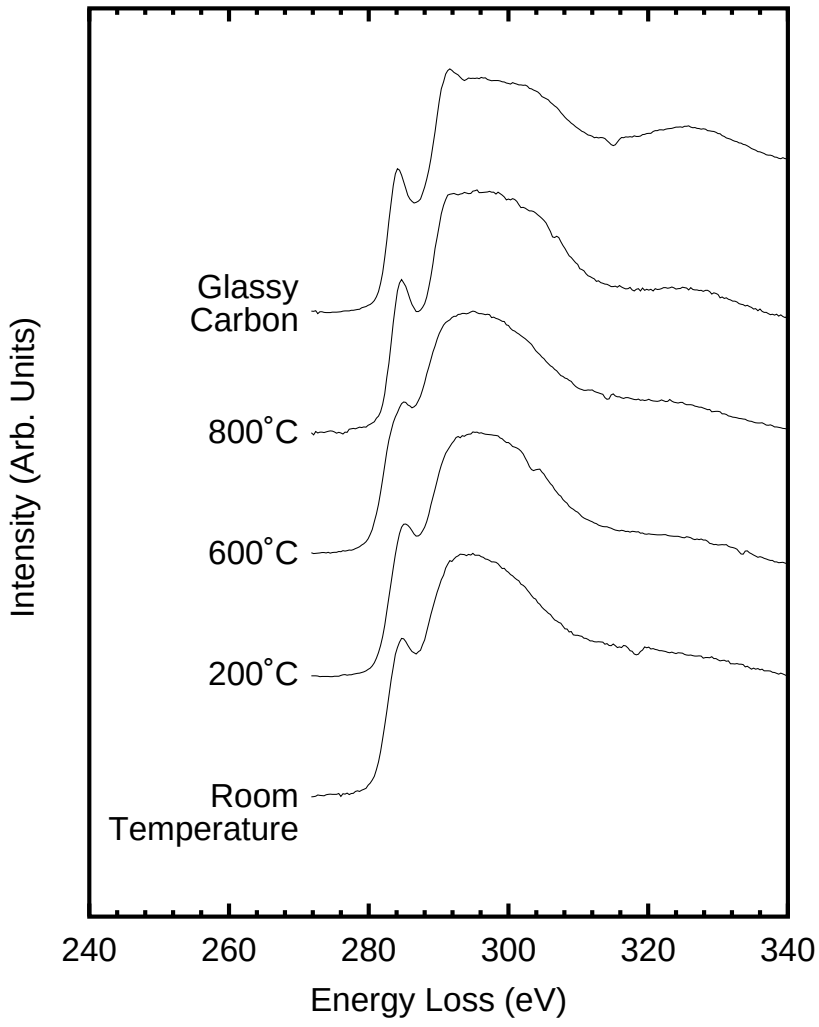

Figure 3.9: The background-subtracted carbon EELS K-edge for glassy carbon, the as-deposited carbon nitride film (CN-31) and the carbon nitride film following annealing to temperatures of 200°C, 600°C and 1000°C.

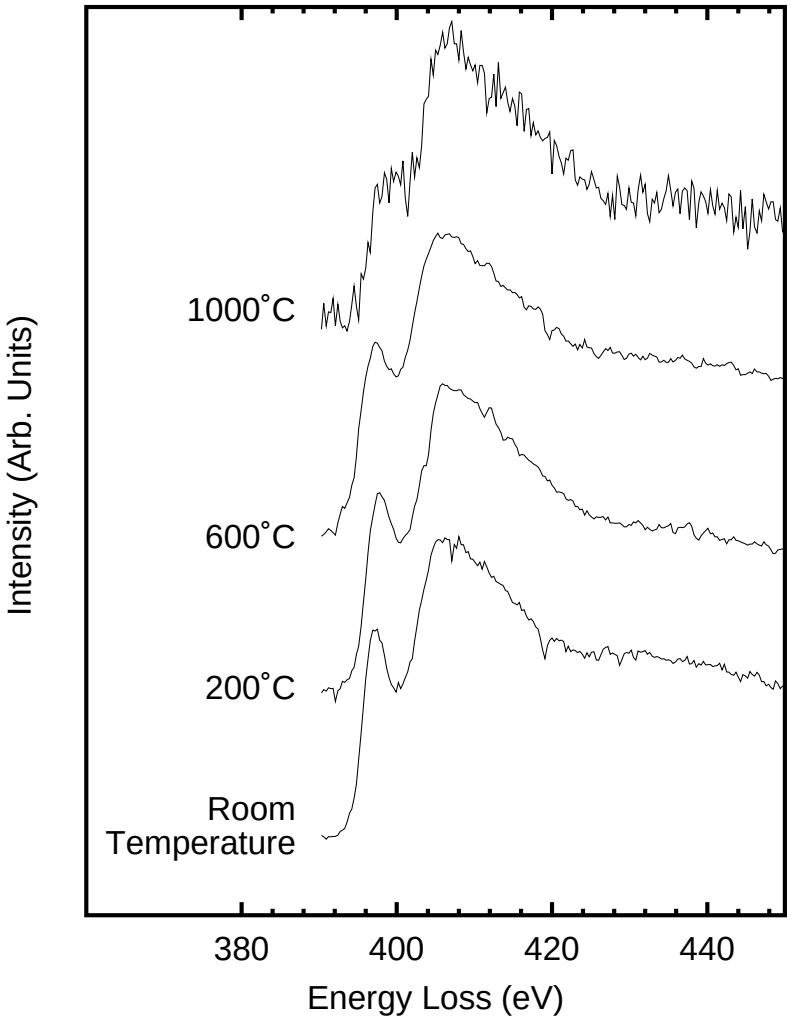

Figure 3.10: The background-subtracted nitrogen EELS K-edge for the as -deposited carbon nitride film and the carbon nitride film following annealing to temperatures of 200°C, 600°C and 1000°C.

3.2.5.1 Comparison to more recent annealing experiments

Recently, work by Bhattacharyya *et al.* [7] has increased the amount of nitrogen incorporated into amorphous carbon nitride films using the cathodic arc. Bhattacharyya *et al.* used a novel technique of linking a Kaufmann N^+ ion source to a filtered cathodic arc. This ensured that the nitrogen gas did not reduce the energy of carbon ions arriving at the substrate, and produced films of high sp^3–carbon content. The high amorphous carbon–sp^3 matrix enabled films of up to 36% nitrogen concentration to be formed. Bhattacharyya found using a combination of Near-Edge X-ray Absorption Fine structure (NEXAFS) and EELS that the increase of nitrogen produced an increase in the number of C=N over C–N bonds, indicating that increasing the nitrogen concentration was allowing nitrogen to "substitute" into a carbon–sp^2–like site. An annealing experiment by Bhattacharyya *et al.* [12] showed a large amount of nitrogen loss at a few hundred degrees Celsius illustrating that nitrogen atoms were only weakly bound in the amorphous carbon matrix, in agreement with the similar reduction in nitrogen concentration at elevated temperatures discussed in the previous Section.

Jiménez *et al.* [13] studied the effect of thermal annealing on carbon nitride deposited by an arcjet by monitoring the C- and N-K Edge Near-Edge X-ray Absorption Fine-Structure (NEXAFS). The $a-$C:N material studied initially had a N/C 1s – σ^* intensity ratio[1] of ≈2. At between 300-400°C almost half the nitrogen had desorbed leaving a remnant of N/C≈1. Examination of the nitrogen 1s – π^* feature by Jiminéz *et al.* concluded that $a-$C:N resembled $a-$C and contained several types of bonding but that carbon-sp^2 was dominant. Interestingly, Jiminéz *et al.* also concluded that C-N bonds within the graphitic framework stabilised the structure, which was thermally more stable than $a-$C, despite changes in C-N bonding while annealing. The results presented earlier in this chapter also concur with the findings of Jiménez *et al.* in that the carbon nitride is a stable phase but has an increasing carbon-sp^2 character with increasing temperature, rather than the evolution of a carbon-only graphitic phase within an a-C:N matrix.

[1] This was not a quantitative measure but rather a ratio of C(1s) and N(1s) intensities.

3.2.6 Energy Filtered Electron Diffraction

In fig (3.11) the energy filtered electron diffraction pattern for the a-C and CN50 materials is shown, collected using the technique described in Section 2.3.4 on page 40. It can be observed that there is an enhancement of the {002} graphite reflection which arises from the layering of the structure in the CN50, indicating that the nitrogen incorporation into the $a-$C network has promoted the formation of layers in the structure. Therefore the carbon nitride network appears closer in structure to glassy carbon than to a-C. It has a predominantly sp^2 network with variable ring size, a greater degree of planarity but with somewhat less sp^3 residual than a-C.

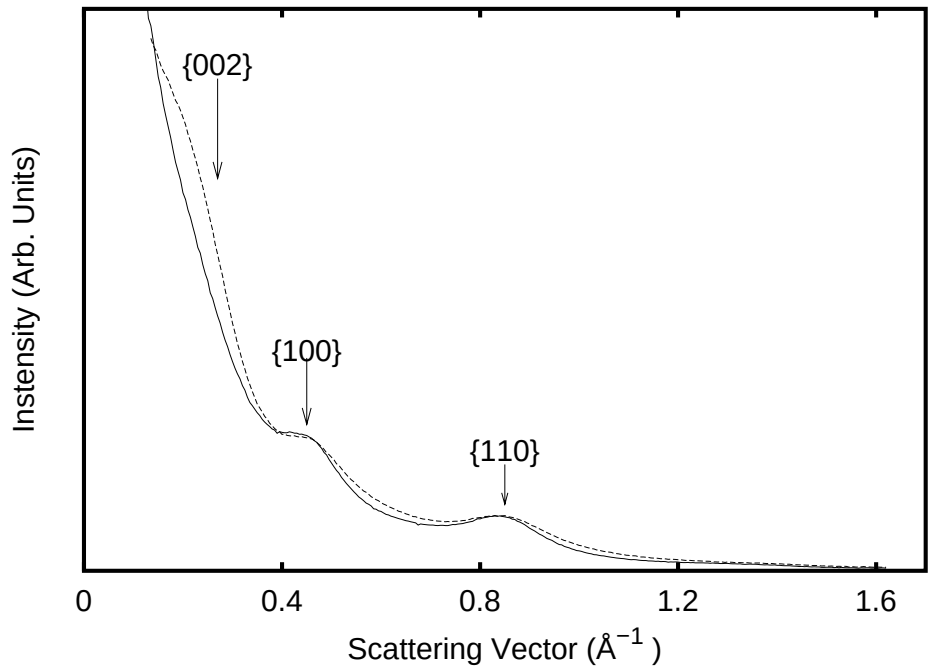

Figure 3.11: Energy Filtered Electron Diffraction Patterns for cathodic arc deposited amorphous carbon (a-C) in the presence of argon and CN50 (dotted line). The diffraction peaks indicated as {002}, {100} and {110} refer to the d-spaces in graphite.

3.2.7 Experimental Radial Distribution Function, G(r)

The fig (3.12) shows experimentally measured G(r) plots (calculated from collected I(s) and transformed using the technique described in Section 2.3.2 on page 38) for unimplanted glassy carbon and the three cathodic arc deposited materials. The first two nearest neighbour distances and the bond angle are shown in Table 3.1. The G(r)

from the *a*-C sample shows an increase in the first nearest neighbour distance (1·48Å) relative to glassy car-

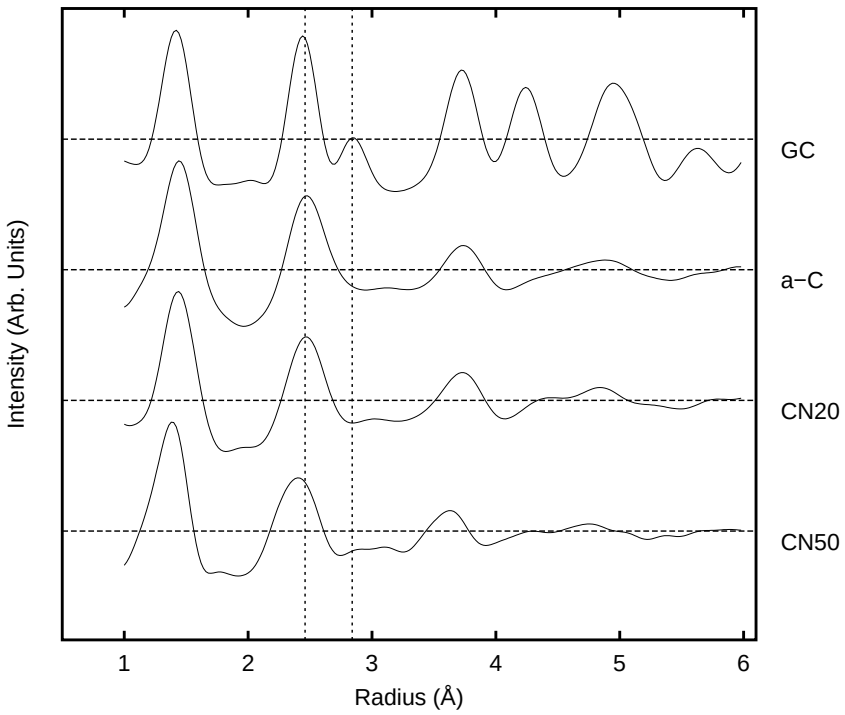

Figure 3.12: Experimentally measured reduced density functions, G(r), for Glassy Carbon (GC), cathodic arc deposited carbon amorphous carbon and carbon nitrides CN50 and CN20. The dotted lines are distances of 2.46 and 2.84Åwhich are characteristic of sp^2 bonded carbon planes.

bon (1·42Å), due to a small proportion of diamond-like bonds (1·55Å) and broadening due to bond angle disorder from five- and seven-membered rings [5]. Compared to *a*-C, the nitrogen containing materials have a shorter bond length and a bond angle of approximately 120°, very close to the angle expected for sp^2 bonded hexagonal layers. Since C=N bond lengths are somewhat shorter than C-C (aromatic) distances (see Table 3.2 on page 78), it is expected that insertion of nitrogen into a primarily sp^2 bonded network such as *a*-C would cause a shortening of the average inter-atomic distances. The similarity in bond angle and bond length in glassy carbon indicates a structural similarity. In fact, there is evidence of some degree of in-plane ordering as occurs in glassy carbon, since peaks in the CN50 $G(r)$ at 2·46Å and 2·84Å are characteristic of sp^2 bonded hexagonal layers.

Material	C-C bond length (Å)	C-N bond length (Å)	Reference
Graphite	1.42	...	[14]
Benzene	1.40	...	[14]
$a-$C	1.44	...	[15]
Pyrazine	1.34	1.34	[14]
Pyrimidine	1.39	1.34	[14]
Pyridine	1.39	1.34	[14]

Table 3.2: Bond lengths in selected ring structures containing nitrogen and carbon. Where possible C-C single bonds and C-N single bonds have been listed [14]

3.2.8 Calculated Radial Distribution Functions, G(r)

The G(r) functions were calculated for a number of proposed crystalline C_3N_4 structures using the eqn(2.10) with a cluster of approximately 80,000 atoms. These are plotted in fig (3.13). The nearest neighbour bond-lengths and bond angles are listed in Table 3.3.

Clearly from a comparison of bond lengths and bond angles contained in Table 3.3, the experimental data for the $a-$C:N films does not fit any of the proposed models for crystalline materials based of C_3N_4. The experimental data of CN50 and CN20 fits the calculated G(r) of a single sheet of graphite based on the formula CN only if some weakening of the in-plane order is allowed for so that the peaks at 2·46Å and 2·84Å are broadened. This result supports the proposition that the structure of the films is largely graphite-like with rings containing both nitrogen and carbon atoms.

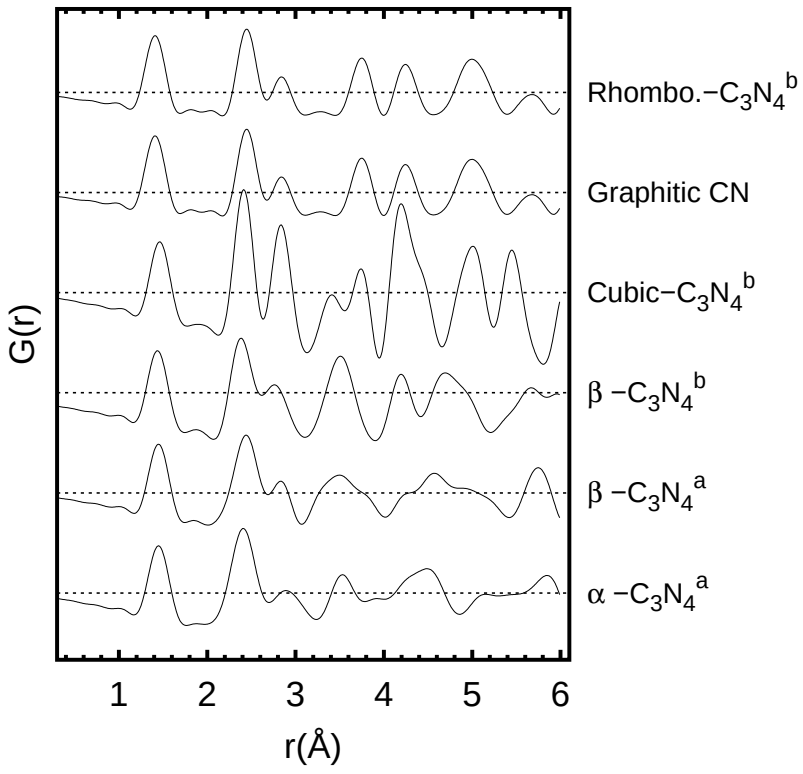

Figure 3.13: Theoretically calculated reduced density, G(r) for various crystalline carbon nitrides as listed in Table 3.3 from ^{a} Guo and Goddard [16] and ^{b} Liu and Wentzcovitch [17].

			Near. Neighbour Distances (Å)		
	Structure	Bond Angle	1st	2nd	3rd
(a)	graphitic (CN)	121°	1.41	2.45	2.84
(b)	rhombohedral C_3N_4[17]	123°	1.34	2.36	3.36
(c)	cubic-C_3N_4[17]	111°	1.46	2.41	2.84
(d)	β-C_3N_4 [17]	112°	1.44	2.38	2.76

Table 3.3: Measurements from the calculated reduced density functions for (a) a single sheet of graphite with 50% of carbon atoms replaced by nitrogen, (b) rhombohedral, (c) cubic and (d) β- crystalline C_3N_4 structures.

3.2.9 Infra-Red Spectra of $a-$C:N

The infra-red absorption spectra of the CN50 and a-C samples are shown in fig (3.14). The a-C sample shows a featureless spectrum except for an absorption peak at 2325 cm^{-1} assigned to C≡C stretching. The graphitic carbon (G band) from 1100–1700cm^{-1} and the disordered carbon network (D band) visible in Raman spectroscopy are both forbidden in IR for $a-$C and $ta-$C, and are therefore absent in the spectra shown for $a-$C.

The $a-$C:N sample, however, shows significant IR activity, with the CN50 sample showing significant absorption in the 1200–1600 cm^{-1} region, with the D and G regions clearly active. Han and Feldman [18] argued that substituting a N atom in place of a C atom in an sp^2 bonded carbon network will induce strong IR activity; consequently the increased absorption in the 1200-1600 cm^{-1} region between the $a-$C and $a-$C:N samples is expected if the N atoms are bonded into an sp^2 carbon network. Kaufmann *et al.* [5] argues that in pyridine-like rings, the inclusion of nitrogen atoms breaks the symmetry, activating the G band.

The peak at the higher energy of 2200 cm^{-1} and the weaker absorption peak at 2350cm^{-1} are attributed to C≡C and C≡N triple bond stretching modes [18, 19, 20]. These are a clear indicator that sp bonded carbon and nitrogen atoms are present in both $a-$C and $a-$C:N networks, though the relative amounts present are not known

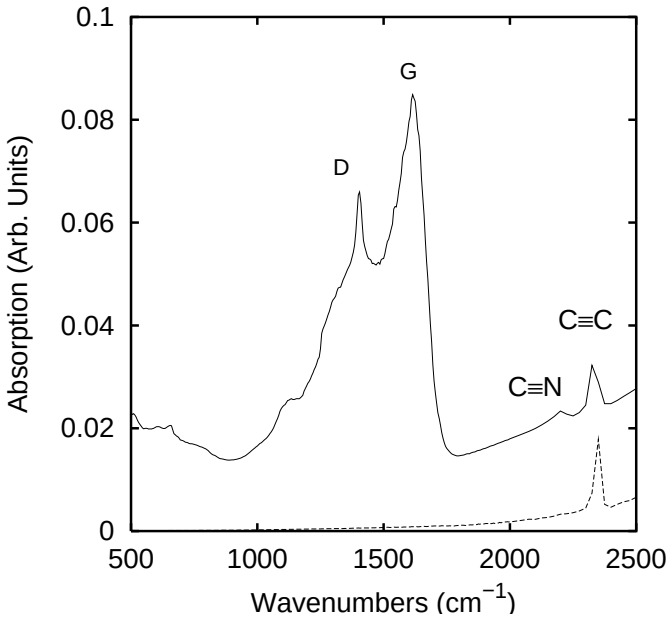

Figure 3.14: Infra-red Absorption Spectra of cathodic arc deposited materials (i) CN50 and (ii) a-C deposited in argon ambient. Carbon triple bonded to carbon and nitrogen absorption peaks identified from Han and Feldman [18].

because of variations in the general oscillator strength.

Similar IR absorption spectra showing the D and G bands, and C≡N absorption at 2200cm^{-1} were measured in ion-beam-sputtered samples of $a-$C:N by Kobayashi *et al.* [21].

3.2.10 Raman Spectra of $a-$C:N

The Raman spectra of cathodic arc deposited CN50, $a-$C, nitrogen implanted glassy carbon and unimplanted glassy carbon samples is shown in fig (3.15). From the figure it can be seen that unimplanted glassy carbon shows two Raman active peaks, labelled D and G on the figure. The D and G peaks are the Disordered carbon and Graphitic carbon peaks respectively [4]. From the figure it can be seen that the $a-$C sample is mostly graphitic (as also shown by EELS), and that the nitrogen implanted glassy carbon (to a dose of 5×10^{17}N/cm^2) results in a similar spectrum, indicating the implanted layer is amorphous. There is also a slight D peak in the implanted sample which corresponds to a peak in the vibration density of states of graphite and therefore

its presence implies the presence of significant fraction of sp^2 bonded material with reasonable in plane order.

The Raman spectrum for CN50 sample shows a larger D peak than the implanted sample indicating superior in-plane ordering compared to both the $a-$C and implanted samples. This emergence of the D peak is supported by the $I(s)$ measurement which shows the CN50 sample has enhanced $\{002\}$ ordering.

It should be noted that the Raman spectra of the cathodic arc deposited $a-$C:N samples was very difficult to measure due to poor sample stability while it was being irradiated, even at the lowest beam intensities.

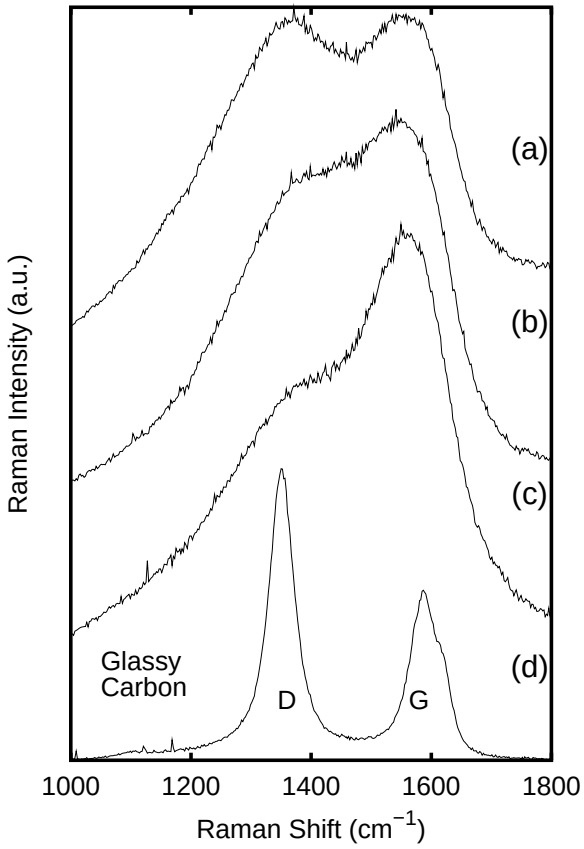

Figure 3.15: Raman Spectroscopy is used to determine the amount of graphitic and disordered sp^2-bonded carbon in (a) CN50, (b) nitrogen implanted glassy carbon to a dose of 5×10^{17}N/cm^2, (c) cathodic arc deposited $a-$C and (d) an unimplanted glassy carbon sample.

3.3 CVD deposition of Diamond and Carbon Nitrides

As explained in Chapter 1, there are other methods of depositing carbon nitrides, including chemical vapour deposition (CVD). The purpose of this work was to emulate the work of Chen *et al.* [22] who had reported the successful deposition of crystalline carbon nitrides using a similar technique.

CVD deposition of diamond involves the high-temperature breakdown of reactive gases (methane and hydrogen) into a plasma using an energy source including a hot tungsten filament [22], a microwave magnetron to excite the plasma and inductive or capacitive coupling. The presence of hydrogen promotes the formation of carbon–sp^3 or diamond-like sites, required for the formation of extremely hard phases of carbon nitrides. If either nitrogen (N_2) [23] and/or ammonia gas [24] is added to the mixture, it should be possible to deposit crystalline or amorphous carbon nitrides. In this section, a brief description of the materials deposited by hot-filament and microwave CVD will be presented.

3.3.1 Hot Filament CVD

In the first experimental series using the hot-filament assisted CVD (HF-CVD), the amount of hydrogen/methane/nitrogen gas introduced into the system was gradually changed from 99%/1%/0% to 0%/1%/99% at which point bias-assisted depositions were also made using a filament to substrate bias of -150 and -300V. A general observation was that as amount of hydrogen was reduced, the deposition rate and substrate temperature dropped down to 640° using a 1%CH_4/99%N_2 gas mixture. Under -300V bias tungsten was deposited onto the substrate from the filament.

When viewed through an SEM, the 99% H_2/1%CH_4/0%N_2 sample revealed faceted twinned diamond crystals as seen in fig (3.16)(a). With an increase/decrease in nitrogen/hydrogen gas, the deposition rate dropped significantly until for the same deposition time, the crystallites no longer formed facets, and were reduced to porous clumps on the surface as seen in fig (3.16)(d) barely 5μm in size.

When the high nitrogen gas mixture samples were analysed using energy dispersive

spectroscopy (EDS), no nitrogen was found for any of the samples deposited using HF-CVD. This is shown in fig (3.17) which shows the EDS spectrum from a sample of HF-CVD diamond deposited from a $CH_4/H_2/N_2$ gas mixture. The inset to fig (3.17) is an EDS spectrum collected from cathodic arc deposited $a-$C:N (CN50) with a small nitrogen peak. The oxygen K_α peak in the figure present because the sample is a thin-film which had been exposed to air for some months and had absorbed a surface layer of oxygen.

Because the purpose of this study was to find high-nitrogen content crystalline carbon nitrides, to check that the carbon was not absorbing the nitrogen x-rays, the EDS spectra for carbon nitrides were simulated using CASINO.

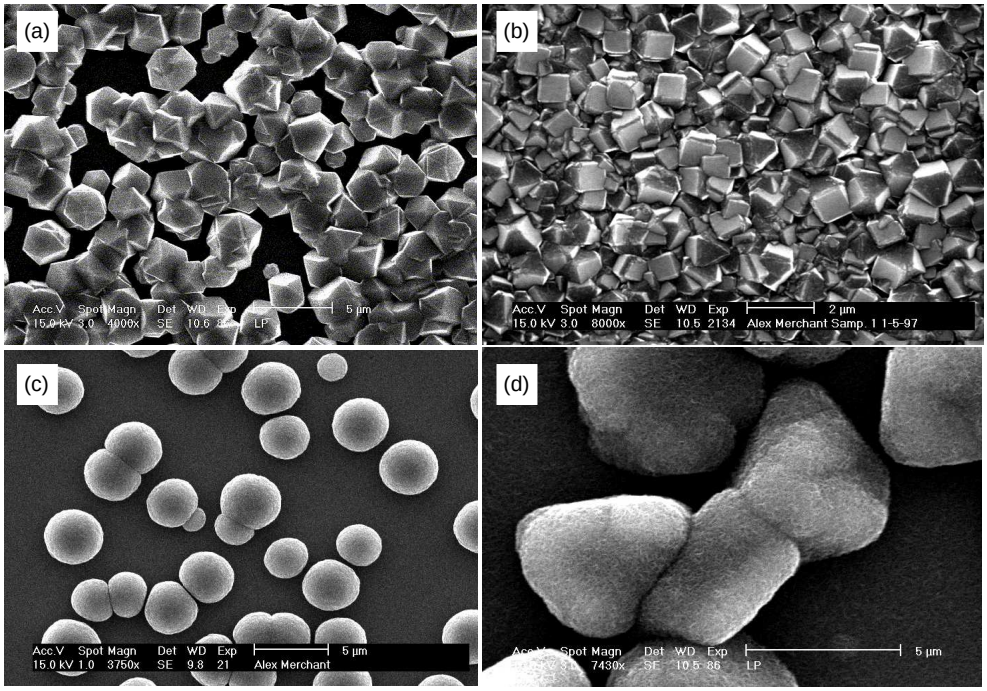

Figure 3.16: Scanning electron micrographs of diamond deposited using (a) hot-filament and (b) microwave CVD, and (c),(d) two carbon crystalline materials deposited under similar conditions.

3.3.1.1 Modelling EDS spectra using CASINO

CASINO is a single scattering Monte **CA**rlo **SI**mulation of electro**N** trajectory in s**O**lid specifically designed for low-energy beam interaction in a bulk or thin foil. The program

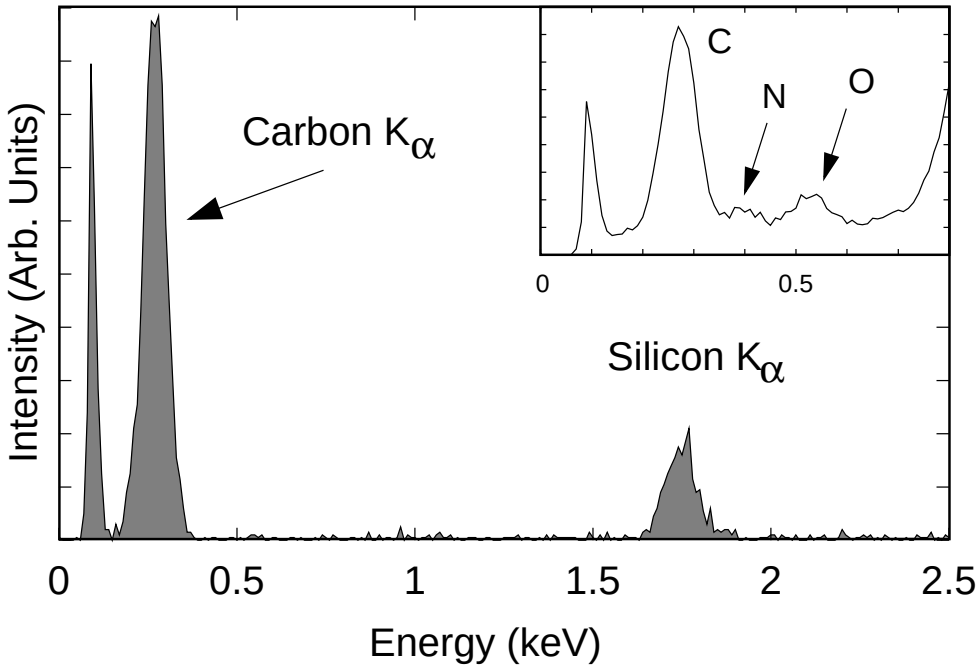

Figure 3.17: EDS spectrum for diamond deposited onto Silicon substrates using HF-CVD with a $CH_4/H_2/N_2$ gas mixture showing only carbon and silicon characteristic x-rays and no nitrogen. Inset is the EDS spectrum from cathodic arc deposited $a-$C:N showing a N peak of diminished amplitude due to absorption from the carbon matrix.

uses tabulated Mott elastic cross sections experimentally determined stopping powers. To test the efficiency of nitrogen x-ray detection in a carbon matrix a hemispherical inclusion of radius 2.5μm of density 3.55g/cm^3 was placed in a silicon matrix (chosen as all samples were deposited onto silicon substrates, and the silicon x-rays would not contaminate the carbon and nitrogen signals). The results of the study are shown in Table 3.4 for an ultra-thin window EDS detector.

These results of these simulations showed firstly, that if the sample were of sufficient density and size, all x-rays would be confined to the carbon nitride inclusion and there should be no silicon x-rays. Secondly it showed that the deeper the penetration of the electron beam (higher kV), the lower the nitrogen signal-to-background. Thirdly it showed that at low N concentrations (<10%) the nitrogen x-ray signal would be difficult to detect due to the large relative background as shown in Table 3.4.

For the EDS spectra shown in fig (3.17), the height of the nitrogen peak shows there

Voltage (kV)	C at.%	N at.%	I_C/B_C K_α	I_N/B_N K_α	I_{Si}/B_{Si} K_α
5	90	10	599/127	37/43	0/0
10	90	10	1072/362	26/53	0/0
15	90	10	1174/563	18/54	0/0
5	50	50	309/134	255/64	0/0
10	50	50	522/363	235/102	0/0
15	50	50	534/537	168/107	0/0
5	40	60	243/136	334/71	0/0
10	40	60	406/366	352/126	0/0
15	40	60	400/522	244/131	0/0

Table 3.4: The detection of nitrogen in a carbon matrix using EDS is difficult because the carbon will absorb nitrogen x-rays. Using CASINO[25], the integrated intensities for C and N K_α signals from carbon nitrides at different microscope kV can be simulated.

is appreciable absorption by the carbon and the EDS spectrometer window of nitrogen x-rays.

However the CASINO modelling showed if there were high nitrogen content ($> 10\%$) crystalline material it would be easily measurable by EDS. The conclusion of the hot-filament CVD deposition was that nitrogen was not incorporated into the deposited material at a level comparable to the cathodic arc deposited material. No regions of high nitrogen content were observed and therefore no crystalline carbon nitride materials of the composition C_3N_4 were formed on a scale visible to SEM analysis.

3.3.2 Hot-filament bias-assisted CVD from another laboratory

During this course of study, a sample of bias-assisted HF-CVD deposited material from Chen *et al.* [22, 26, 27] at the Chinese Academy of Sciences was analysed. Chen *et al.* had reported numerous successes in synthesising crystalline carbon nitride with bias-assisted (-500V) hot-filament CVD using N_2/CH_4 feed gases on silicon and nickel substrates. Chen *et al.* presented mostly SEM results on the morphology of

crystalline regions as deposited using the technique, which were not conclusive, as discussed previously in Chapter 1. The sample provided was analysed using SEM, firstly to look for regions high nitrogen content. The sample was found to contain only carbonaceous regions.

3.3.3 Microwave assisted CVD

In similar experiments to the HF CVD depositions, a microwave–assisted CVD deposition system was used in an attempt to deposit carbon nitride materials. Using the deposition system described in Section 2.2.2 on page 31, and a gas mixture of H_2/CH_4 1% diamond was deposited for six hours using a constant 600W magnetron. The resulting film is shown in fig (3.16)(b) which shows clear $< 100 >$ faceting of the diamond crystals showing this is the preferred growth direction. There is significantly less twinning of crystals compared to the HF-CVD grown diamond.

The addition of nitrogen to the microwave-assisted CVD system caused the reduction of faceting on diamond crystal surfaces similar to the HF-CVD deposition. But in the high nitrogen gas mixtures (20% N_2), instead of depositing diamond, silicon was sputtered from the substrate and reacted with the nitrogen gas in the plasma and was redeposited as silicon nitride. An SEM micrograph and EDS spectrum of this silicon nitride material is shown in fig (3.18), where the nitrogen K_α x-ray can be clearly seen. No other materials deposited contained any nitrogen (to limit of measurement) using EDS.

3.4 Reactively sputtered $a-$C:N

The sample of reactively sputtered carbon nitride from Chowdhury *et al.* [28, 29] was prepared for CTEM using IBT (See Section 2.3.8) and examined in the CTEM and STEM as shown in fig(3.19). Chowdhury *et al.* [29] has previously reported on electron diffraction showing "nano"–crystalline areas with crystallography consistent with the β-C_3N_4 phase. Using RBS and Raman spectroscopy, Chowdhury *et al.* [29] had found only carbon, nitrogen, and trace levels of hydrogen present.

A normalised EELS C-K and N-K edge for the sample can be seen in figs(3.20 &3.21)(c). The samples contain (35±5)% nitrogen. An energy filtered electron diffraction pattern was collected and the $G(r)$ for the sample was calculated. This G(r) is shown in fig(3.22) in comparison to CN50 in which the first two nearest neighbour peaks are at 1.40Å and 2.44Å with average bond angle of 121° which was very similar to values for CN50 in Table3.1. The G(r) and EELS results suggests this material is a very similar material to the cathodic arc deposited $a-$C:N and high dose nitrogen implanted glassy carbon. No crystalline carbon-nitride regions were found in the sample, and the analysis by EELS showed the bonding was consistent with an sp^2-carbon matrix. The experimental amorphous carbon nitride and theoretical crystalline carbon nitride spectra will be presented in Section 5.5 on page 154.

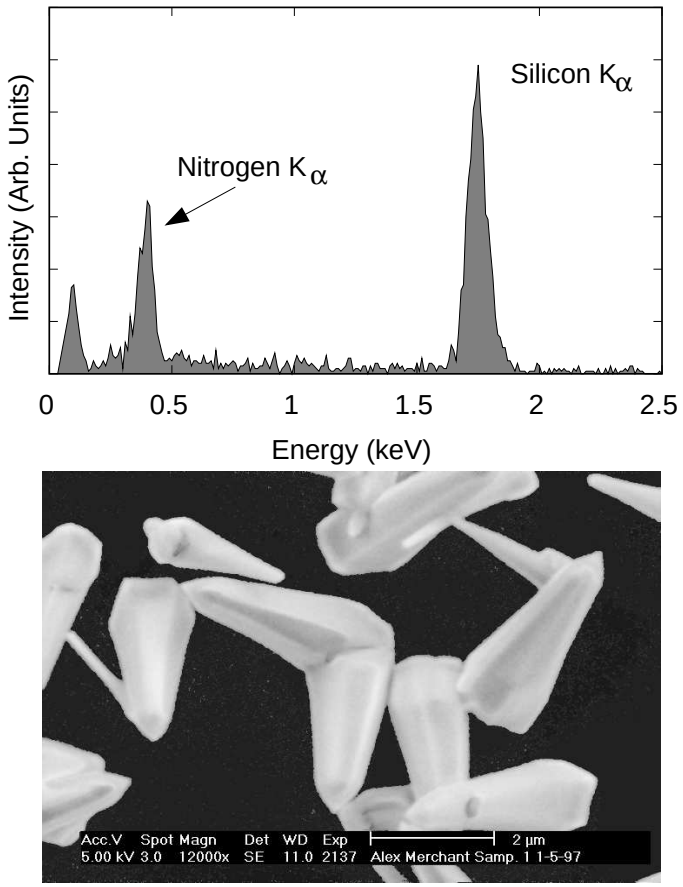

Figure 3.18: Scanning electron micrographs and an EDS spectrum of silicon nitride deposited using microwave CVD, silicon sputtered from the substrate is combined with nitrogen and deposited.

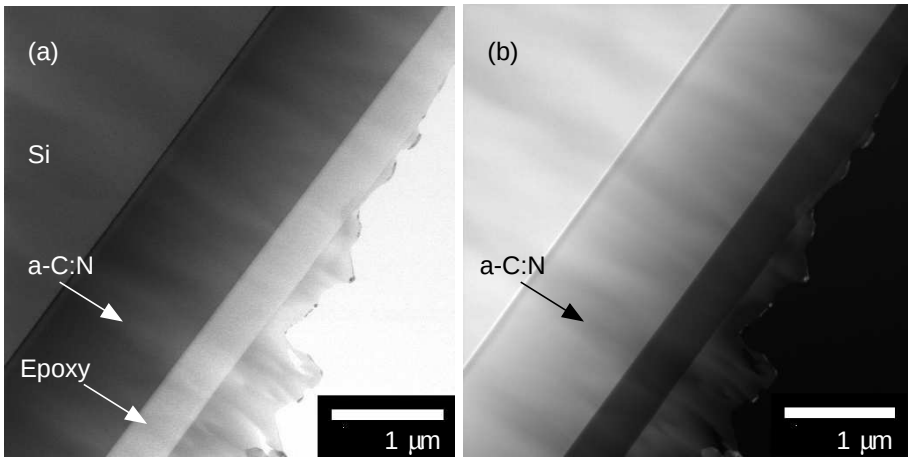

Figure 3.19: STEM Micrographs of reactively sputtered amorphous carbon nitride in (a) bright field and (b) dark field modes. In the image, top left is the Silicon substrate, followed by the film and then an epoxy layer.

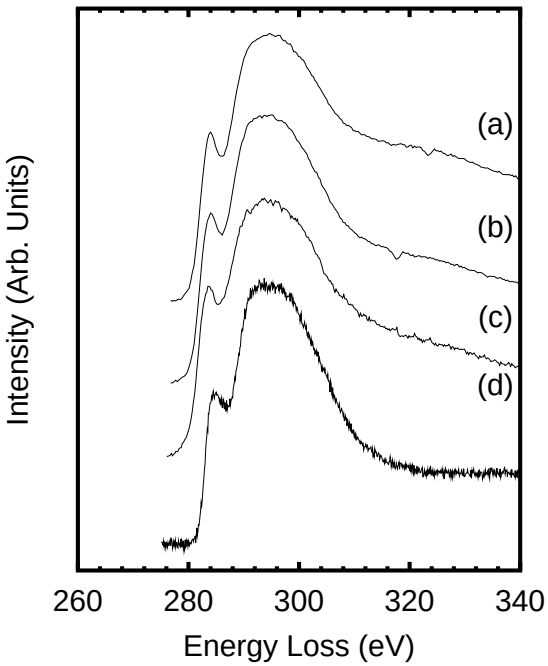

Figure 3.20: EELS Carbon K-edge for three carbon nitride samples deposited by three different techniques, (a),(b) cathodic arc samples CN50 and CN20, (c) reactively sputtered carbon nitride and (d) plasma-assisted CVD carbon nitride.

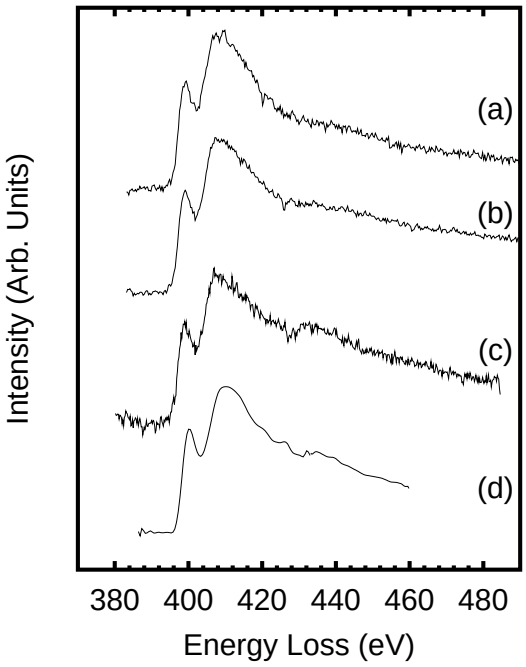

Figure 3.21: EELS nitrogen K-edge for three carbon nitride samples deposited by three different techniques, (a),(b) cathodic arc samples CN50 and CN20, (c) reactively sputtered carbon nitride and (d) plasma-assisted CVD carbon nitride (smoothed by an sbezier function to remove noise, spectrum has also been deconvoluted the remove multiple scattering).

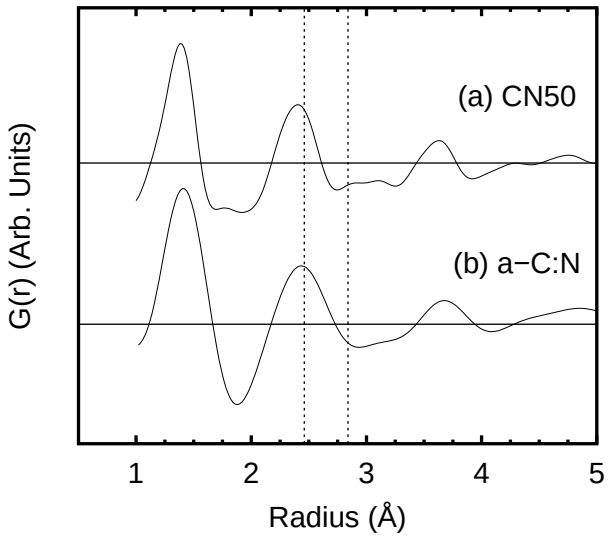

Figure 3.22: Radial distribution function G(r) of reactively sputtered amorphous carbon nitride compared to cathodic arc sampleCN50, the dotted lines are 2·46Å and 2·84Å are characteristic of sp^2-carbon bonded hexagonal layers.

3.4.1 Plasma-assisted CVD

A plasma-assisted CVD deposited carbon nitride sample from Institut für Festkörper- und Werkstofforschung, Dresden, a research laboratory in Germany was also analysed. This sample was the basis of work which was published as by Grüger et al. [30] showing micro-diffraction of small crystallites matching the diffraction pattern of crystalline carbon nitride. Our aim was to determine the elemental composition of the micro-crystallites. The majority of the sample consisted of thick amorphous carbon nitride material (shown in fig(3.23)), for which the typical EELS C-K edge and N-K edge are shown in figs(3.20 & 3.21)(d). The region sampled for the spectra were particularly thick and were over an amorphous carbon support film which is why the deconvoluted N-K edge spectrum appears broader in the 1s – π^* and 1s – σ^* regions of (d) than the other samples. An EELS elemental analysis of the carbon nitride region showed the region contained (30±5)% nitrogen. We found no evidence of micro-crystallites mentioned by Grüger et al. [30].

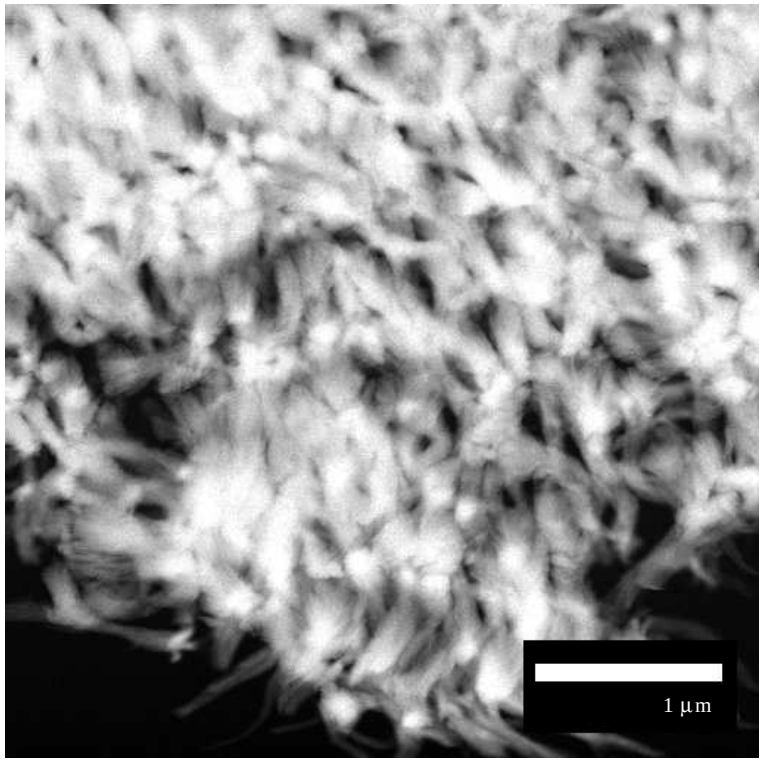

Figure 3.23: A STEM micrograph of Plasma-assisted CVD deposited carbon nitride from Grüger *et al.* (1997).

3.5 Structural Model for cathodic arc $a-$C:N

The amorphous carbon nitride materials deposited using cathodic arc, reactive sputtering and nitrogen implantation into glassy carbon all appear to share a common bonding environment for the carbon and nitrogen atoms. When compared carbon K-edge to carbon K-edge, and nitrogen K-edge to nitrogen K-edge, the shapes in the implanted glassy carbon sample, reactively sputtered sample and cathodic arc-deposited materials are almost identical, strongly suggesting that on average, each carbon and nitrogen atom they have a similar bonding environment in each material. All the materials studied had a nitrogen concentration of between 20–33%($\pm$5%) and a predominantly sp^2 carbon matrix with nitrogen π bonding present. The G(r) for the CN50 sample and the reactively sputtered sample is very similar with strong correlation between the first, second and third nearest neighbour peaks.

The materials deposited using bias-assisted HF and microwave-assisted CVD methods did not contain the same amount of nitrogen as the PVD techniques. Using bias-asssited HF CVD, at a bias of -300V, it was found the tungsten from the filament was deposited onto the substrate. With no H_2 gas present in microwave–assisted CVD, substrate material was ablated, reacted with the nitrogen feed gas, and was re-deposited as silicon nitride.

The carbon nitride material deposited using plasma-assisted CVD in Section 3.4.1, while containing large amounts of nitrogen, again appeared similar to the PVD techniques, as shown by the ELNES of the carbon and nitrogen K-edges.

3.5.1 Saturation of nitrogen in $a-$C:N

An extended network of sp^2 bonded carbon & nitrogen atoms (sp^2-CN) cannot support a concentration of nitrogen above a certain level. This level is logically determined by three mechanisms: the first is if two nitrogen atoms bond they are volatile and will be lost from the structure. The second mechanism is the formation of volatile C-N molecules, and the third is the reduction of connectivity in the network due to network-terminating sites of π-bonded $-\ddot{\mathrm{N}}=$ sites.

The concept of nitrogen "saturation" in an amorphous sp^2–carbon matrix is also supported by RBS spectra of nitrogen implanted glassy carbon of McCulloch [1]. These spectra show the C edge and Gaussian-like N profile characteristic of an implanted species. At the irradiation dose of $5{\times}10^{17}\mathrm{Ncm}^{-2}$ and above, the N profile becomes flat topped and some oxygen is introduced into the implanted layer. The flat topped impurity distribution indicates that a saturation N concentration has been reached, calculated from the RBS spectra to be $5 \times 10^{17}\mathrm{Ncm}^{-2}$ which corresponds to a peak [N]/[C] ratio from the implanted layer was calculated (from the RBS spectra) to have a value of 0·35 (26%[N]) to 0·45 (31%[N]).

Further evidence for the saturation of the level of nitrogen in $a-$C:N is the SEM images in fig(3.24) which shows the surface of the glassy carbon sample implanted to a dose of $5{\times}10^{17}\mathrm{N}^{+}$ cm^{-2}. Note that this image has been tilted by 60°. It can be seen from this image that the implanted surface contains small pin holes, approximately 50 nm in diameter. These features were not observed in glassy carbon samples irradiated with other ion species and are clearly different from the blisters formed on the glassy carbon surface due to the presence of buried inert gas bubbles [15]. The appearance of small holes on the surface of the N irradiated sample may be the result of the nitrogen containing gas escaping from the implanted layer through the surface leaving small holes. Weich *et al.* [31] noted that in density functional tight binding simulations of 1.5 and 2.00 $\mathrm{g/cm}^3$ $a-$C:N at high nitrogen concentrations that network terminating CN groups and even N_2 dimers were present, which limited the bonded nitrogen concentration in the simulation to about 40%.

The annealing experiment also supports the concept of "saturation" as it shows sample CN50 contains both "loosely" bonded nitrogen (e.g. gaseous nitrogen trapped in voids) and nitrogen bonded within a sp^2-carbon/nitrogen amorphous network. As the anneal temperature is increased to 200°C the loosely bound nitrogen is driven from the amorphous structure and the nitrogen concentration decreases to 26%. The structure at this point consists of sp^2 bonded carbon and nitrogen atoms, probably in the form of distorted rings with up to 2 nitrogen atoms per 5-, 6- or 7-membered ring. Then, as the temperature increases beyond 400°C the carbon atoms within the carbon-nitride

structure begin to rearrange themselves into graphite-like hexagonal carbon, driving nitrogen out of the network.

3.5.1.1 Evolution of Nitrogen from Cathodic Arc $a-$C:N

As discussed earlier, the as-deposited carbon nitride material consists of sp^2 bonded carbon-nitrogen rings which are limited to about 2 nitrogen atoms per six-membered-ring or a nitrogen concentration of about 33%. The limit of 2 nitrogen atoms per ring can be explained by the fact that the introduction of nitrogen into sp^2 bonded carbon rings removes one bond between the ring and the local environment by the formation of a lone pair. Therefore, rings containing more than 2 nitrogen atoms are likely to be volatile and therefore readily lost from the network. Evidence for the ejection of nitrogen volatile has been observed from features on the surface of nitrogen implanted glassy carbon as seen in fig (3.24) and also by Withrow *et al.* [32] who also found a saturation of nitrogen content in nitrogen implanted glassy carbon despite a doubling of nitrogen dose from 5×10^{17}cm^2.

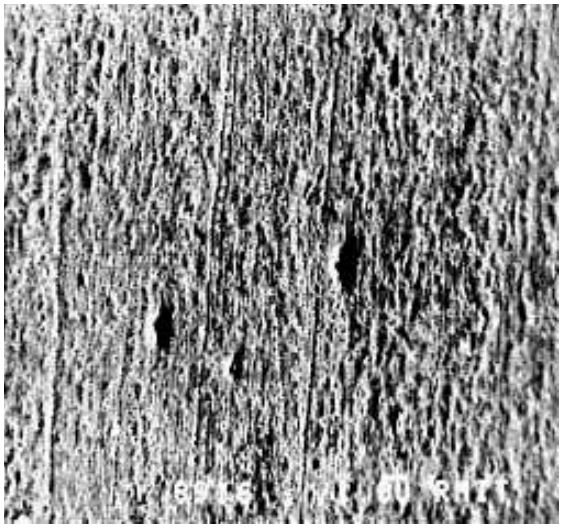

Figure 3.24: SEM images of the surface of the glassy carbon sample implanted to a dose of 5×10^{17}Ncm^{-2} tilted to show pin-holes (not present before implantation). These could be produced by nitrogen gas escaping. Reproduced with Permission McCulloch (1994).

3.5.2 Comparison to phase-diagram of $a-$C:N

The cathodic arc deposited carbon nitride corresponds neatly to the phase diagram of Kleinsorge *et al.* [33] as shown in Chapter 1 in fig. (1.4). In the diagram Kleinsorge predicts that the structure of $a-$C:N will alter from an sp^2-matrix to a more fullerene-like structure with increasing deposition temperature and increasing nitrogen content. In Section 3.2.6 the energy filtered electron diffraction pattern shows increased ordering in the $a-$C:N structure which may be indicative of this type of structure. The annealing "path" on fig (3.25) shows how the structure of the $a-$C:N is expected to shift, decreasing the nitrogen concentration, and enhancing the sp^2-carbon fraction. Hellgren *et al.* [34] found that for dc magnetron sputtered films a saturated level of nitrogen was lower for higher temperatures ($\approx 350°$). Hellgren ascribed this to a nitrogen saturation, due to a maximum nitrogen level of one per aromatic ring, which is consistent with fig (3.4).

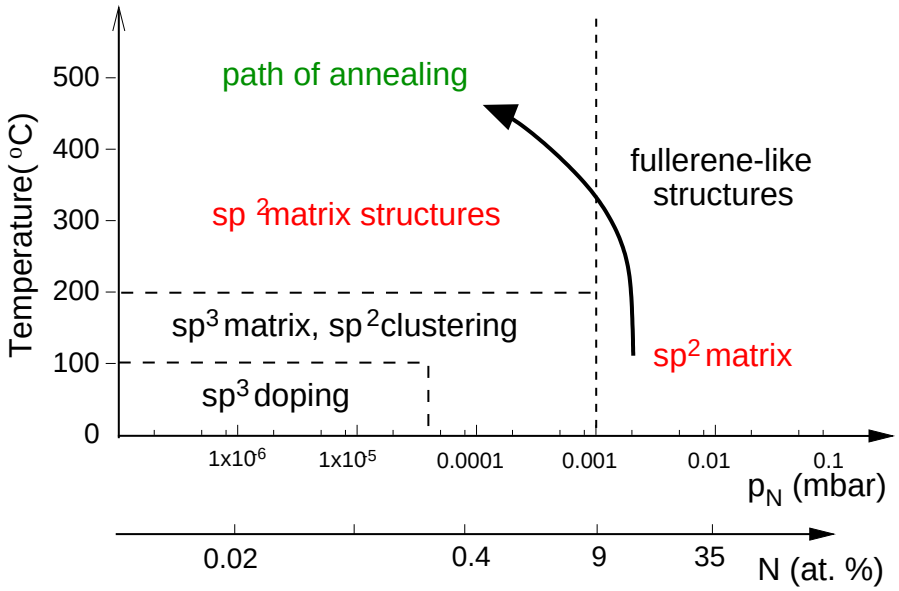

Figure 3.25: A phase diagram for amorphous carbon nitride following Kleinsorge *et al.* [33] and after Hellgren *et al.* [34] showing path of annealing experiment.

3.6 Conclusions

The structures of the amorphous carbon nitride materials produced by cathodic arc deposition, reactive sputtering, plasma-assisted CVD and nitrogen implantation of glassy carbon were analysed and found to be remarkably similar. These samples shared a like bonding environment for carbon and nitrogen atoms, and where comparison was available, shared the same structural properties.

It is proposed that this structure is predominantly sp^2-carbon bonded with the nitrogen atoms incorporated into the carbon network. It is also proposed that the amount of nitrogen present in the amorphous carbon network reaches a saturation level caused by the predominance of 5-, 6- and 7-membered rings in the structure This saturation level is 33% N, or a maximum of two nitrogen atoms in a six-membered ring.

The effects of annealing on the structure of cathodic arc deposited amorphous carbon nitride films were investigated for anneal temperatures up to 1000°C. There was no evidence for the presence of crystallites containing nitrogen within the film structure over this temperature range. It was found that annealing the carbon nitride films results in the graphitisation of the film structure which drives nitrogen out of the network.

Throughout our experimental studies no evidence was found for a crystalline structure resembling β-C_3N_4, nor for an amorphous derivative of the same stoichiometry. This included samples obtained from other research laboratories deposited using several different techniques.

Bibliography

[1] D. G. McCulloch, Ph.D. thesis, RMIT University, 1994.

[2] R. F. Egerton, 2nd ed. (Plenum Press New York, 1996).

[3] R. O. Dillon, J. A. Woollam, and V. Katkanant, Physical Review B **29,** 3482 (1984).

[4] D. G. McCulloch, E. G. Gerstner, D. R. McKenzie, S. Prawer, and R. Kalish, Physical Review B **52,** 850–857 (1995).

[5] J. H. Kaufman, S. Metin, and D. D. Saperstein, Physical Review B **39,** 13053–13060 (1989).

[6] I. Jiménez, R. Gago, J. M. Albella, D. Cáceres, and I. Vergara, Physical Review B **62,** 4261–4264 (2000).

[7] S. Bhattacharyya, M. Lubbe, and F. Richter, Journal of Applied Physics **88,** 5043–5049 (2000).

[8] I. Shimoyama, G. Wu, T. Sekiguchi, and Y. Baba, Physical Review B **62,** R6053–R6056 (2000).

[9] V. S. Veerasamy, J. Yuan, G. A. J. Amaratunga, W. I. Milne, K. W. R. Gilkes, M. Weiler, and L. M. Brown, Physical Review B **448,** 17954–17959 (1993).

[10] J. Stohr, *NEXAFS Spectroscopy* (Springer-Verlag Berlin, 1992).

[11] C. A. Davis, D. R. McKenzie, Y. Yin, E. Kravtchinskaia, G. A. J. Amaratunga, and V. S. Veerasamy, Philosophical Magazine B **69,** 1133–1140 (1994).

[12] S. Bhattacharyya, M. Hietschold, and F. Richter, Diamond and Related Materials **9,** 544–547 (2000).

[13] I. Jiménez, W. M. Tong, D. K. Smith, B. C. Holloway, M. A. Kelley, P. Pianetta, L. J. Terminello, and F. J. Himpsel, Applied Physics Letters **74,** 2620–2622 (1999).

[14] *CRC Handbook of Chemistry and Physics*, 73rd ed., D. R. Lide, ed., (CRC Press Inc. Ann Arbor, 1992–93).

[15] D. G. McCulloch, S. Prawer, A. Hoffman, and D. K. Sood, Nuclear Instrumentation and Methods **8081,** 1480–1484 (1993).

[16] Y. Guo and W. A. Goddard, Chemical Physics Letters **237,** 72–76 (1995).

[17] A. Y. Liu and R. M. Wentzcovitch, Physical Review B **50,** 10362–10365 (1994).

[18] H. X. Han and B. J. Feldman, Solid State Communications **65,** 921–923 (1988).

[19] D. G. McCulloch and S. Prawer, Journal of Applied Physics **78,** 3040 (1995).

[20] M. Y. Chen, D. Li, V. P. Dravid, Y. W. Chung, M. S. Wong, and W. D. Sproul, Journal Vacuum Science Technology **A11,** 521–524 (1993).

[21] S. Kobayashi, K. Miyazaki, S. Nozaki, H. Morisaki, S. Fukui, and S. Masaki, J. Vac Sci and Technol. A **14,** pp777–780 (1996).

[22] Y. Chen, L. P. Guo, and E. G. Wang, Modern Physics Letters B **10,** 615–617 (1996).

[23] P. W. May, P. R. Burridge, C. A. Rego, R. S. Tsang, M. N. R. Ashfold, K. N. Rosser, R. E. Tanner, D. Cherns, and R. Vincent, Diamond and Related Materials **5,** 354–358 (1996).

[24] V. Baranauskas, S. F. Durrant, M. C. Tosin, A. C. Peterlevitz, B. B. Li, and S. G. Castro, Thin Solid Films **356,** 157–161 (1999).

[25] P. Hovington, D. Drouin, and R. Gauvin, Scanning **19,** 1–14 (1997).

[26] Y. Chen, L. P. Guo, F. Chen, and E. G. Wang, Journal of Physics Condensed Matter **8,** L965 (1996).

[27] Y. Chen, L. P. Guo, and E. G. Wang, Phil. Mag Letters **75,** 155 (1997).

[28] A. K. M. S. Chowdhury, M. A. Monclus, and D. C. Cameron, Thin Solid Films **356,** 85–88 (1999).

[29] A. K. M. S. Chowdhury, D. C. Cameron, M. S. J. Hashmi, and J. M. Gregg, Journal of Materials Research **14,** 2359–2363 (1999).

[30] H. Grüger, D. Selbmann, E. Wolf, and A. Leonhardt, Surface and Coatings Technology **97,** 109–113 (1997).

[31] F. Weich, J. Widany, and T. Frauenheim, Phys. Rev. Lett. **78,** 3326 (1997).

[32] S. P. Withrow, J. M. Williams, S. Prawer, and D. Barbara, Journal Applied Physics **78,** 3060–3065 (1995).

[33] B. Kleinsorge, A. C. Ferrari, J. Robertson, W. I. Milne, S. Waidman, and S. Hearne, Diamond and Related Materials **9,** 643–648 (2000).

[34] N. Hellgren, M. P. Johansson, E. Broitman, L. Hultman, and J.-E. Sundgren, Physical Review B **59,** 5162–5169 (1999).